UNIVERSITÀ POLITECNICA DELLE MARCHE

FACOLTÀ DI INGEGNERIA

Corso di Laurea in Biomedical Engineering

Engineering of Medical Devices

Cost-effective biocompatible materials for the bioprinting of 3D colloidal scaffolds

Relatore:

Prof.ssa Alida Mazzoli

Tesi di Laurea di:

Francesco Marucci

Correlatore:

Prof.ssa Francesca Luzi

Prof.ssa Pasquapina Ciarmela

A.A. 2023/2024

Contents

Abstract

In recent years, significant advancements have been made in the field of three-dimensional (3D) bioprinting, particularly in the development of bioinks for a wide range of applications, including regenerative medicine and tissue engineering. This study aims to address the need for standardized, cost-effective bioinks by developing a bioink formulation using natural, biocompatible polymers. Specifically, nine different alginate-based hydrogels were formulated, with two pure alginate and seven incorporating varying concentrations of gelatin, collagen, and xanthan gum. These formulations were selected to optimize mechanical properties, cell compatibility, and printability for 3D bioprinting applications. The crosslinking process was achieved using an 80 mM $CaCl_2$ solution for 15 minutes, which ensured immediate stiffness after printing, a key factor in preserving the shape and stability of the printed structures. In the initial phase of the study, 3D constructs were printed using the CellInk BioX printer without cells, allowing for evaluation of the hydrogels ability to form stable structures. Scanning electron microscopy (SEM) and rheological analysis were employed to further investigate the structural and mechanical properties of the hydrogels. The results demonstrated that the 10%(w/v) alginate scaffold successfully maintained its structural integrity and exhibited superior rheological properties for extrusion printing, indicating its potential as a viable bioink. The second phase of the study focused on bio-fabrication, in which Leiomyosarcoma cell lines were inoculated into the alginate matrix to assess cellular behavior within the 3D constructs. This process made at the Department of Experimental and Clinical Medicine of UNIVPM involved detailed analysis of cell proliferation, morphology, and viability, with subsequent microscopy and DAPI staining confirming positive cell growth over time. The findings revealed that the 10% alginate bioink supported cell proliferation and spheroid aggregation, demonstrating its potential as cost-effective and viable platforms for tissue engineering, regenerative medicine, and future research applications.

1 Introduction

3D bioprinting has emerged as a revolutionary technology in the field of tissue engineering and regenerative medicine, offering the potential to fabricate complex, functional tissue constructs that can mimic natural tissues. Among the various bio-inks available, alginate-based bio-inks have gained significant attention due to their excellent biocompatibility, tunable mechanical properties, and ease of gelation [1]. Alginate, a naturally derived polysaccharide, is particularly valued for its ability to form hydrogels under mild conditions, which is essential for maintaining cell viability during the printing process. For successful extrusion-based 3D bioprinting, the selection of a suitable bio-ink is crucial and hinges on three primary factors: biocompatibility, printability, and mechanical properties. Biocompatibility ensures that the bio-ink can support cell survival, proliferation, and differentiation [4]. Printability involves the ability of the bio-ink to be extruded smoothly and maintain structural integrity post-printing. Mechanical properties are vital for ensuring that the printed constructs have sufficient strength and stability to support cellular activities and withstand physiological conditions. In this study, we developed nine different alginate solutions by varying the concentrations of collagen, gelatin, and food thickener (ThickenUp) This approach aimed to create a tunable bio-ink platform that can be adapted for a wide range of soft tissue engineering applications, including bone, vascular, and adipose tissue engineering [2,3]. By modifying the composition of the alginate-based bio-inks, we sought to optimize their biocompatibility, printability, and mechanical properties to meet the specific requirements of different tissue types. The systematic investigation of these alginate-based bio-inks will provide insights into their performance and suitability for various applications. This work contributes to the ongoing efforts in the field to develop versatile and cost-effective bio-inks that can facilitate the advancement of 3D bioprinting technology and its applications in creating functional tissue constructs in a standardized methodology.

1.1 Alginate Hydrogels

Alginate, a naturally occurring anionic polymer derived from brown seaweed, is widely used to develop a variety of composites for tissue engineering (TE), drug delivery, wound healing, and cancer therapy. This sustainable and renewable biomaterial exhibits several remarkable properties, including high biocompatibility, low toxicity, cost-effectiveness, and mild gelation when combined with divalent cations (e.g., Ca2+). Alginate-based biomaterials can be fabricated into different forms such as hydrogels, foams, sponges, fibers, microspheres, and microcapsules using various techniques[5]. Among these, alginate hydrogels are particularly valuable for applications such as tissue repair and regeneration due to their supportive matrix or delivery system capabilities[6]. These biomaterials have been employed in tissue engineering (TE) and regenerative medicine (RM) in forms like hydrogels/gels, films, fibers, gauzes, foams, and wafers [7]. Their numerous advantages include high porosity and surface area , cost-effectiveness and ease of manufacture, strong absorption capacity and facilitated cell migration among others[8]. The most common method for preparing alginate gels involves ionic crosslinking with multivalent cations such as Ca2+ [10]. Optimizing manufacturing conditions with a focus on solubility, reactivity, and characterization is crucial for developing effective alginate-based composites for TE-RM applications. Overall, these renewable and sustainable biomaterials can be hybridized or modified to design next-generation alginate-based composites with multifunctional properties.

1.2 Biofabrication: bioprinting

Biofabrication is an emerging research area and includes the creation of tissue constructs with a hierarchical architecture. The definition of biofabrication is the generation of biologically functional products in an automated manner with structural organization by using bioactive molecules, living cells, and cell aggregates, such as micro-tissues, biomaterials, or hybrid cell-material constructs via bioassembly or bioprinting, and subsequent tissue maturation processes[11]. More recently, 3D bioprinting has emerged as a novel biofabrication method, offering significantly improved control over the architecture of the fabricated tissue constructs with high reproducibility endowed by the automated deposition process [12,13]. Essentially, bioprinting allows for the fabrication of 3D tissue constructs with pre-programmed structures and geometries containing biomaterials and/or living cells (the bioink). The main 3D bioprinting modalities are laser-assisted bioprinting (LaBP), inkjet bioprinting/droplet bioprinting, and extrusion-based bioprinting (Fig.1). Moreover, employing multi-head deposition systems (MHDSs) enables the concurrent or sequential extrusion of various materials

during the printing process. In these methods, 3D constructs are programmed in a computer-aided design/computer-aided manufacturing (CAD/CAM) system.

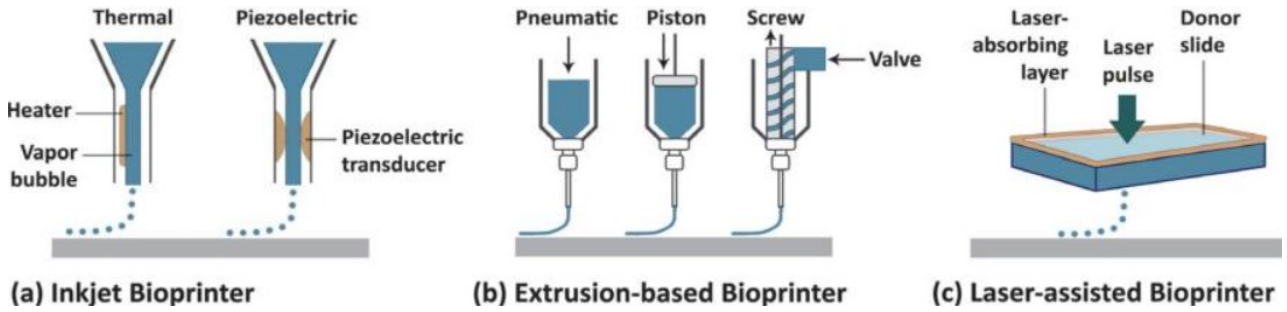

Fig.1: 3D bioprinting technologies. (a) Inkjet/droplet bioprinting. (b) Extrusion-based bioprinting. (c) Laser-assisted bioprinting.

1.3 Extrusion-Based Bioprinting

Extrusion-based bioprinting is one of the most common techniques in 3D bioprinting, where bioink is extruded through a nozzle to create continuous filaments, layer by layer, forming 3D structures. This method is particularly suitable for printing with high viscosity bioinks and allows precise control over the deposition of cells and materials [14]. Important to notice that the biggest drawback is that cells are exposed to shear stress when passing through the nozzle and pressure while in the syringe prior to extrusion, both of which can decrease cell viability and function. [15]

1.4 Bioinks

Bioinks are formulations of biomaterials and living cells, sometimes with growth factors or other biomolecules (Fig.2) . Successful printing of constructs and their subsequent applications rely on the properties of the formulated bioinks, including the rheological, mechanical, and biological properties, as well as the printing process. An ideal bioink must exhibit optimal physicochemical properties, including suitable mechanical, rheological, chemical, and biological traits[16]. These characteristics should enable: (i) the formation of tissue constructs with sufficient mechanical strength and durability, while maintaining tissue-like mechanics, (ii) controlled gelation and stabilization to facilitate the bioprinting of structures with high shape fidelity; (iii) biocompatibility and, where necessary, biodegradability, closely mimicking the tissue's natural microenvironment; (iv)

adaptability for chemical modifications to meet specific tissue requirements; and (v) scalability for large-scale production with minimal batch-to-batch variation[17]. As the development of an optimal cell-laden bioink formulation is critical for successful bioprinting, a wide range of natural and synthetic biomaterials with unique features have been employed as bioinks [18]. Furthermore, there is an urgent need for standardized bioink formulations that can be applied across various bioprinting applications.

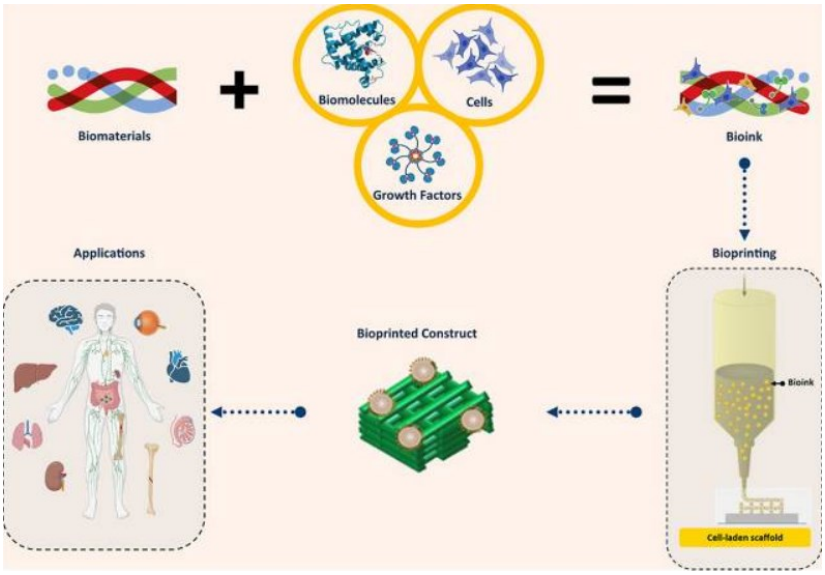

Fig.2: Graphic scheme of bio printed construct from a bioink

1.5 Crosslinking

Alginate is a sort of polyanionic polysaccharide composed of α-L-Gulonuronic acid (G unit) and β-D-Mannuronic acid (M unit), which are linked by β-1,4-glycosidic bonds [19]. Bio-based hydrogels can be synthesized using various chemical and ionic crosslinking techniques, as well as other methods such as photopolymerization and exposure to radiation (e.g., gamma rays or microwaves)[20]. Chemical crosslinking involves the creation of covalent bonds during the reaction between a polymer or monomer and a crosslinking agent like polyethylene-glycol-diacrylate (PEGDA), typically in the presence of an initiator such as ammonium, potassium, or sodium persulfate[21]. On the other hand, ionic crosslinking occurs through interactions with divalent or multivalent ions like Ca2+, Cu2+, Fe2+, or Al3+. Alginates are among the most well-known polymers that can be crosslinked through ionic interactions[22]. This class of polysaccharides forms a three-dimensional structure when exposed to divalent ions at room temperature and under physiological conditions (pH 5.2–5.5). The

gelation process of ionically crosslinked alginates is particularly intriguing because it leads to the formation of a three-dimensional structure known as the "egg box" model (Fig.3). In this model, divalent ions bind to guluronic acid via ionic bonds, allowing the guluronic block of one polymer chain to connect with adjacent G blocks [22,23].

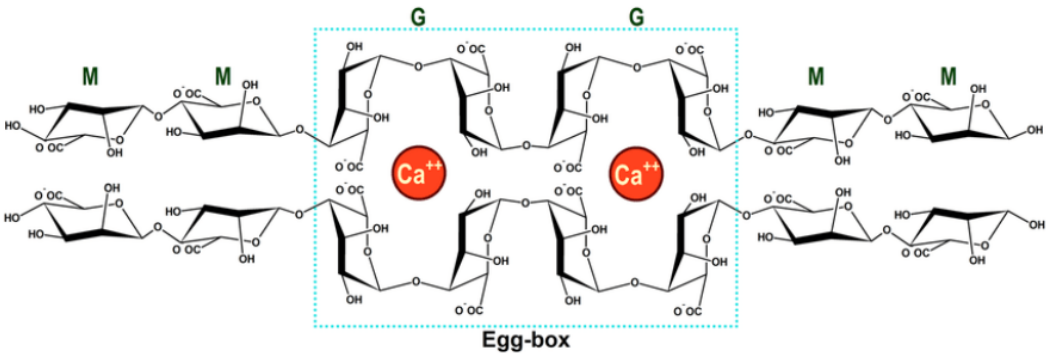

Fig.3: Schematic of "Egg-box" structure in alginate hydrogel crosslinked with calcium ions.

2 Materials and methods

2.1 Cellink: BioX bioprinter

The BIO X bioprinter (Fig.4) represents an innovative platform designed for flexibility and ease of use, offering a highly intuitive bioprinting experience facilitated by advanced software accessible via a large touchscreen display. This system is engineered to produce precise tissue constructs, enabling applications in drug discovery, and accelerating the development of new treatments by potentially reducing the need for animal testing and improving early-stage efficacy evaluations. Technically advanced (Fig.5), the BIO X is capable of fabricating constructs with any cell type, making it versatile for creating a wide range of tissue targets. It supports the incorporation of specialized cells such as chondrocytes for cartilage, fibroblasts for dermal applications, and hepatocytes for drug screening models. The system also enables the creation of vascular networks within constructs and can rapidly generate advanced disease models with the addition of stellate cells. The inclusion of Intelligent Printheads (iPH), the first of their kind in the world, further expands the range of materials and applications, allowing researchers to push the boundaries of bioprinting. Environmental control is a key feature of the BIO X, which is equipped with dual high-power fans that channel air through a dual-filtration system, including a prefilter for larger particles and a HEPA H14 filter that removes 99.995% of unwanted particles and microorganisms. This Clean Chamber™ technology is enhanced by UV-C germicidal lights, positive air pressure, and a design featuring rounded edges to prevent particle entrapment, ensuring a sterile environment throughout the printing process. Users can initiate Clean Chamber before beginning their experiments to maintain full sterility around the print area. Moreover, the BIO X offers precise temperature control, with a printhead temperature range of 4°C to 250°C and a printbed temperature range between 4°C and 65°C. This allows for the bioprinting of a wider range of materials and cell types, particularly temperature-sensitive ones like collagen and gelatin, expanding the possibilities for tissue engineering and regenerative medicine applications [https://www.cellink.com/bioprinting/bio-x-3d-bioprinter/]. Technical specifications are reported in Tab.1.

Fig.4: Inkredible+ Bio X bioprinter

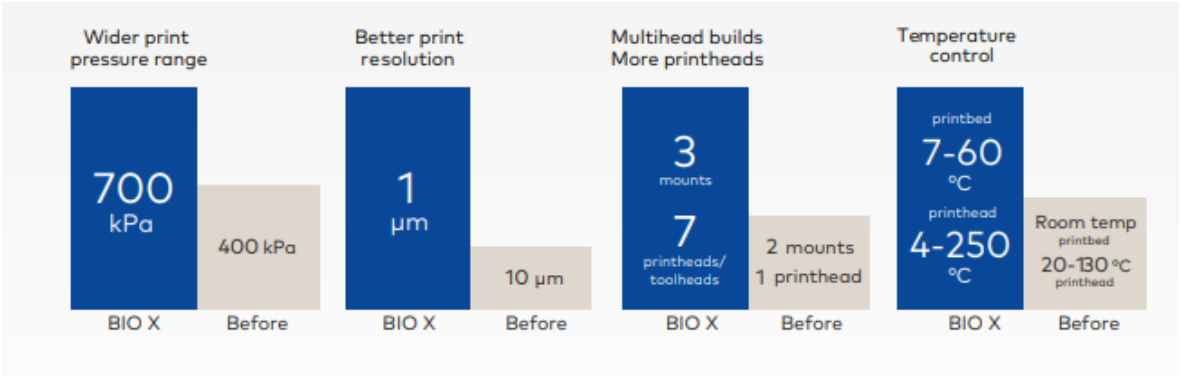

Fig.5: Comparative analysis of key specifications between the BIO X bioprinter and other versions

Table 1. Technical specifications of the Cellink Bio X bioprinter

Specification	Details
Outer Dimensions (L x W x H)	477 mm x 441 mm x 365 mm
Weight	18 kg
Build Volume	130 mm x 90 mm x 70 mm
Build Surface Compatibility	Multi-well plates, petri dishes, glass slides
Resolution XY	1 μm
Layer Resolution	1 μm
Pressure Range (Internal Pump)	0-200 kPa
Pressure Range (External Air Supply)	0-700 kPa
Printhead Slots	3
Photocuring Sources (Built-in)	365 nm, 405 nm, 485 nm, 520 nm
Printbed Temperature Range	4-65 °C
Printhead Temperature Range	4-250 °C (printhead specific)
Filter Class, Chamber Air-flow	HEPA 14
UV-Sterilization	UV-C (275 nm) 20 mW output
Calibration Options	Manual and Automatic
User Interface	Integrated Display, Tablet or Computer
OS Compatibility	Windows
Connectivity	USB Storage, Ethernet Connection
Supported File Formats	.gcode, .stl

2.2 Hydrogels Overview

In this study, sodium alginate, purchased from SaporePuro (ITA), was prepared in distilled water at room temperature. An 80 mM $CaCl_2$ solution (Product number 328257, dry calcium chloride pure powder, Codex®, Carlo Erba, Milan, ITA) was utilized as a cross-linking agent for sodium alginate. To explore the optimal hydrogel concentration that would provide sufficient self-supporting ability, a range of sodium alginate concentrations was tested. Initially, two pure alginate hydrogels were formulated at 8% and 10% (w/v) concentrations. Building upon these, seven additional composite hydrogels were developed by combining alginate with various concentrations of collagen, gelatin from bovine skin type B (Sigma-Aldrich, St. Louis, USA), and Xanthan Gum in the commercial version for food use as ThickenUp Clear (Nestlé, Vevey, Switzerland) (TKU). The compositions can be viewed in Tab.2. These diverse formulations were designed to evaluate the influence of varying concentrations and combinations of these materials on the mechanical properties, printability, and self-supporting capabilities of the hydrogels.

2.2.1 *Gelatin*

Gelatin, produced through the partial hydrolysis of collagen, offers several benefits, including excellent biocompatibility, non-immunogenicity, cell affinity, and complete biodegradability in vivo [24]. Due to its similar composition to collagen, gelatin is widely utilized in tissue engineering applications. Like collagen, gelatin is temperature-sensitive and crosslinks at lower temperatures [24].

2.2.2 *Collagen*

Collagen is a naturally abundant protein in the body, composed of self-aggregating polypeptide chains stabilized by hydrogen and covalent bonds. It is the most used natural material for tissue scaffolds, due to its natural receptors for cell attachment, which enable direct influence on cell adhesion and function [25]. Several types of collagens have been identified, with some being more suitable for bioprinting applications than others [26]. In tissue engineering, the most frequently utilized collagen types include I, II, IV, and V [27], with type I collagen being particularly prevalent in scaffold bioprinting. Moreover, combining collagen solutions with other materials like alginate, gelatin, and HA has been employed to enhance the mechanical properties of bioprinted scaffolds [28].

2.2.3 *Xanthan gum*

Xanthan gum (XG) is a significant microbial polysaccharide, characterized by a linear β-1,4-D-glucose backbone and a trisaccharide side chain. The presence of numerous hydroxyl and carboxyl polar groups on XG chains imparts high hydrophilicity to the polymer. This property allows XG-based hydrogels to exhibit a swelling ratio of up to 26 g/g [29], making them highly effective for the rapid absorption of wound exudates. Additionally, XG chains adopt a five-fold helix conformation stabilized by non-covalent interactions between the hydroxyl and carboxyl groups. These chains can undergo conformational transitions induced by thermal or salt changes [30]. As a result, XG is often combined with other polymers to develop pH- and thermo-responsive carriers for controlled and targeted drug or biomolecule delivery [31], [32].

Table 2. Summary of the nine different hydrogel formulations, highlighting the varying concentrations and combinations of alginate, collagen, gelatin, and Thicken Up used in this study.

Hydrogel	**Composition**	**Concentration (% w/v)**
1	Sodium Alginate	8%
2	Sodium Alginate	10%
3	Sodium Alginate + Collagen	7% + 2%
4	Sodium Alginate + Collagen	8% + 1%
5	Sodium Alginate + Gelatin	9% + 1%
6	Sodium Alginate + Collagen + Thicken Up	6% + 2% + 2%
7	Sodium Alginate + Gelatin + Thicken Up	7% + 2% + 1%
8	Sodium Alginate + Thicken Up	7% + 2.5%
9	Sodium Alginate + Collagen	6.5% + 2.5%

2.3 Hydrogels preparation

In this study, a total of nine distinct hydrogel formulations were prepared, beginning with two sodium alginate-only gels. For this, the required amount of alginate powder was carefully deposited into 10 mL of distilled water at room temperature. The mixture was allowed to hydrate fully (Fig.6) . If the gel exhibited any lack of uniformity after the initial hydration, a magnetic stirrer was employed to ensure complete homogeneity. Following the preparation of the alginate-only gels, the next set of hydrogels incorporated collagen into the formulation (Hydrogels 3, 4, 6, and 9). In these cases, after the alginate was fully hydrated, collagen was gradually added to the mixture while stirring continuously with the magnetic stirrer to ensure even distribution and integration into the gel matrix. For the hydrogels that also contained the thickening agent Thicken Up (Hydrogels 6 and 9), this component was similarly added gradually under constant stirring after the addition of collagen, ensuring a consistent and uniform mixture. For the preparation of the gelatin-containing hydrogels (Hydrogels 5 and 7), a slightly different approach was required. Initially, the gelatin was heated to 60°C using the magnetic stirrer to ensure it was fully dissolved and homogeneously mixed. This temperature was carefully maintained throughout the preparation process, including during the subsequent addition of Thicken Up, if applicable. Once the gelatin was thoroughly dissolved and the Thicken Up was integrated, the alginate was then gradually added to the mixture under continuous stirring to ensure a uniform final gel composition. This methodical approach to hydrogel preparation ensured that each formulation was consistent and suitable for subsequent experimental procedures, such as bioprinting and further analysis.

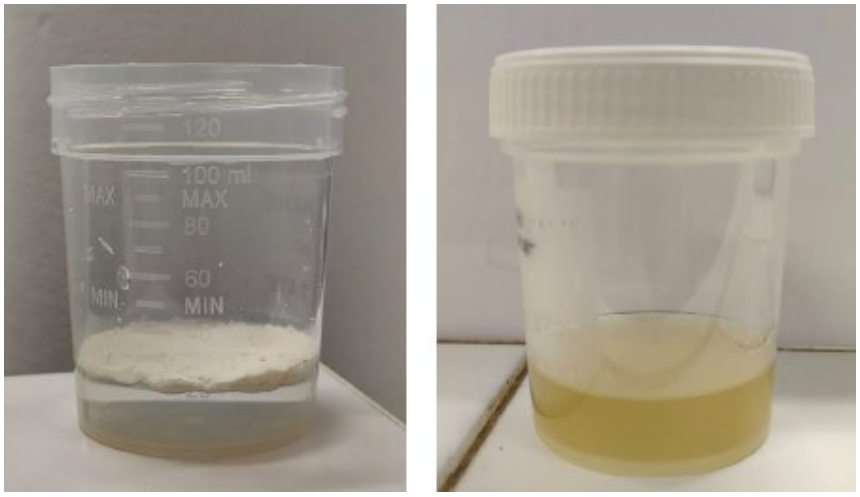

Fig.6: Deposition method for the alginate-only hydrogels

2.4 Hydrogels storage and control

The storage of hydrogels is a crucial factor for ensuring successful bioprinting, primarily to prevent mold formation and bacterial contamination. This is particularly important for hydrogels containing collagen and gelatin, as these materials provide a favorable substrate for microbial growth. To mitigate these risks, all hydrogels were stored at 4°C to inhibit bacterial and mold proliferation. Before beginning the bioink preparation process, the hydrogels were allowed to return to room temperature. Notably, samples stored at room temperature showed a significantly higher spread of mold and bacteria compared to those kept under refrigeration, underscoring the importance of proper storage conditions (Fig.7) .

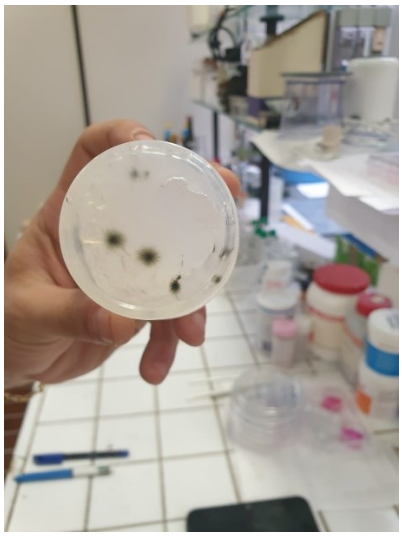

Fig.7: Mold proliferation on hydrogel after 4 days at room temperature

2.4 Cell Line

Leiomyosarcoma cell lines (SK-LMS-1) were obtained from ATCC (Manassas, VA, USA). The cells were cultured in DMEM low glucose (Corning, New York, NY, USA) and added with 10% FBS (Euroclone, Milan, Italy) and 1% antibiotic P/S (Euroclone). The cells were incubated at 37 °C in 95% air and 5% CO2 [33]. Subsequently, cells previously detached from a T75 flask were inoculated with EDTA trypsin (Corning) and counted using the LUNA II automatic counter (Logos biosystem, Annandale, VA, USA). Were used 1× 106 number of cells for each different matrices (TKU/Gel and alginate), and seeded in 6 wells (Falcon, Corning).

2.5 Bioinks preparation

To prepare the cell-laden bioink, cells were first suspended in a control medium (DMEM) to achieve a final concentration of 5×10^5 cells per mL. After selecting the suitable hydrogel constructs, the cell

suspension was mixed with the gel following the standardized procedure proposed by Cellink [https://www.cellink.com/protocols/]. This process was conducted in the Department of Experimental and Clinical Medicine of the UNIVPM, where the cell suspension and hydrogel were carefully combined to avoid the formation of air bubbles. The mixture was gently transferred back and forth between a 1 mL Luer lock syringe containing the cell suspension and the cartridge holding the hydrogel until a homogenous bioink was obtained (Fig.8). The final cell-laden bioink was then loaded into the printing cartridges, ready for the bioprinting process.

Fig.8: Cellink cartridge loaded whit alginate based bioink and Luer lock syringe with cell suspension.

2.6 Printing Process

2.6.1 3D Printing of Hydrogels

In the initial phase of the study, each hydrogel was printed without cells to evaluate their structural integrity and rheological properties. Two types of prints were conducted using the BIO X bioprinter in the Materials Laboratory (SIMAU) at Università Politecnica delle Marche (UNIVPM). The first type involved printing the hydrogels in a 20 mm x 20 mm scaffold-like square pattern (Fig.9a), designed to allow for storage and subsequent control analysis. The second type was a filled version of the same square, used for rheometric analysis to assess the mechanical properties of the hydrogels (Fig.9b). Prior to printing, the bioprinter was carefully calibrated, and parameters such as pressure, printing speed, and extrusion delay were fine-tuned in situ, depending on the viscosity of each hydrogel to ensure optimal print quality.

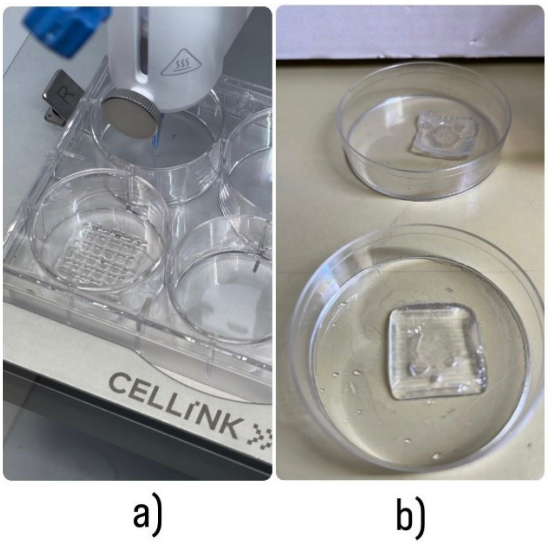

Fig.9: a) 20x20 scaffold-like shape b) filled version for rheological analysis

2.6.1 3D Bioprinting of the Bioinks

After selecting the most suitable hydrogels from the initial tests, these materials were used to create bioinks by mixing them with cells in a controlled environment at the laboratory of the Department of Experimental and Clinical Medicine of the UNIVPM. The cell-laden bioinks were then bioprinted using the INKREDIBLE+ bioprinter from CELLINK. The constructs were printed into 10 mm x 10 mm scaffold structures within six-well dishes (Fig.10). The printer's z-axis and extrusion pressures were meticulously adjusted to achieve optimal results, ensuring precise deposition and maintaining cell viability. This bioprinting process was conducted under sterile conditions to control the integrity of the cells and ensure that the final constructs met the necessary standards for further analysis and potential applications.

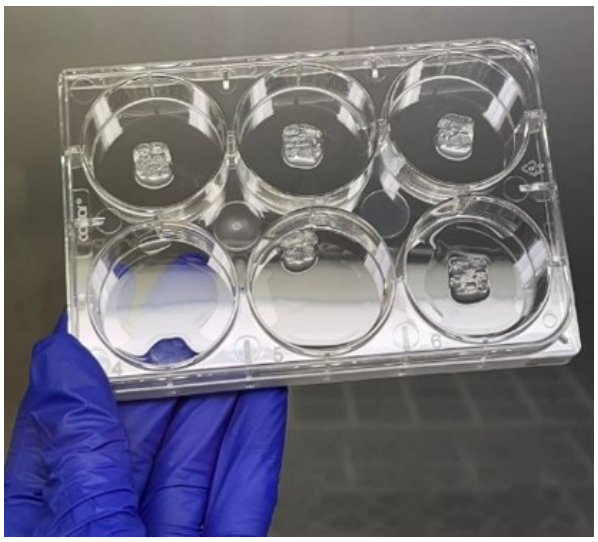

Fig.10: six wells of 10x10 mm bioink scaffolds

2.7 Printing Parameters

In the bioprinting process, maintaining standardized printing parameters is challenging due to the sensitivity of hydrogel viscosity to environmental factors, particularly room temperature. Variations in temperature can cause the hydrogels to become viscous, necessitating real-time adjustments to the printing settings. For each hydrogel, parameters such as pressure, print velocity, and extrusion delay had to be carefully tuned to ensure optimal printing performance. The extrusion pressure varied from 40 kPa to 100 kPa, depending on the density of the hydrogel, with the highest pressure required for the 10% w/v alginate gel. The print velocity ranged between 1 mm/s to 2 mm/s, with adjustments made according to the specific properties of each hydrogel. An initial extrusion delay of 100 ms was generally beneficial for achieving consistent extrusion, especially for more viscous materials. A 22-gauge nozzle with a diameter of 410 μm and a nozzle height of 9.7 mm was used across all constructs. The Tab.3 table provides a comprehensive overview of the printing parameters tailored for each hydrogel, highlighting the need for flexible settings to accommodate varying hydrogel properties.

Table 3. Parameters selected for the bioprinter.

Parameter	Hydrogel 1	Hydrogel 2	Hydrogel 3	Hydrogel 4	Hydrogel 5	Hydrogel 6	Hydrogel 7	Hydrogel 8	Hydrogel 9
Pressure (kPa)	70	90-100	50-60	70-80	90	40-50	60	50	60
Print Velocity (mm/s)	1.5	1.5	1.8	1.5	1.5	2.0	1.8	1.5	1.5
Scaffold Dimension (mm)	20x20	20x20	20x20	20x20	20x20	20x20	20x20	20x20	20x20
Delay Pre-Ext. (ms)	100	100	0	100	100	0	100	100	100
Delay Post-Ex. (ms)	0	0	0	0	0	0	0	0	0
Nozzle Diameter (μm)	410	410	410	410	410	410	410	410	410
Nozzle Height (mm)	9.7	9.7	9.7	9.7	9.7	9.7	9.7	9.7	9.7

2.8 Post Printng Process

After the printing process, the scaffolds were subjected to crosslinking with an 80 mM CaCl2 solution for 15 minutes. This step was crucial as it significantly enhanced the mechanical properties of the sodium alginate films, such as tensile strength and tensile modulus, compared to non-crosslinked films. Tests indicated that scaffolds crosslinked for less than 15 minutes did not achieve the desired mechanical properties; in some instances, these inadequately crosslinked scaffolds completely dissolved within 4 to 5 days, highlighting the importance of the full crosslinking duration (Fig.11).

After the crosslinking, the scaffolds were cultured in a six-well plates containing 5 ml of osteogenic medium, composed of DMEM, 10% FBS, 1% P/S/F, 50 μg ml−1 ascorbic acid (AA), 100 nM dexamethasone (Dex), and 10 mM β-glycerophosphate (β-GP). The culture process was conducted in an incubator set at 37 °C with 5% CO2 to promote cell growth and scaffold maturation for 7 days [29].

Fig.11: not fully crosslinked scaffolds completely dissolved after 5 days

2.9 Rheological Analysis

The rheological properties of the nine hydrogels developed in this study were systematically evaluated and compared to the commercial bioink CELLINK BIOINK. Specifically, alginate hydrogels at concentrations of 8% and 10% w/v, as well as ThickenUp/gelatin/collagene blends were examined at a bioprinting temperature of 25°C using an MCR 702e Anton-Paar rheometer (Graz, Austria) (Fig.12). The tests were conducted using plane–plane geometry with a 25 mm diameter upper plate and a 1 mm gap. Oscillatory shear measurements were performed to assess the elastic (G′) and viscous (G″) moduli, representing the stored and dissipated energy during one deformation cycle. These measurements were conducted across an oscillation frequency (ω) range from 0.1 rad/s to 100 rad/s, with a constant strain (γ) of 0.1%, which falls within the linear viscoelastic range. The loss tangent (tanδ = G″/G′) was calculated to provide insight into the viscoelastic characteristics of the samples. Additionally, the shear viscosity (η) was measured as a function of shear rate ($\dot{\gamma}$) under stationary shear flow conditions, with $\dot{\gamma}$ ranging from 0.01 s−1 to 1000 s−1. These rheological tests were performed without adding DMEM medium to the samples, allowing for direct comparison with CELLINK BIOINK, similar to the procedure followed for other hydrogel preparations.

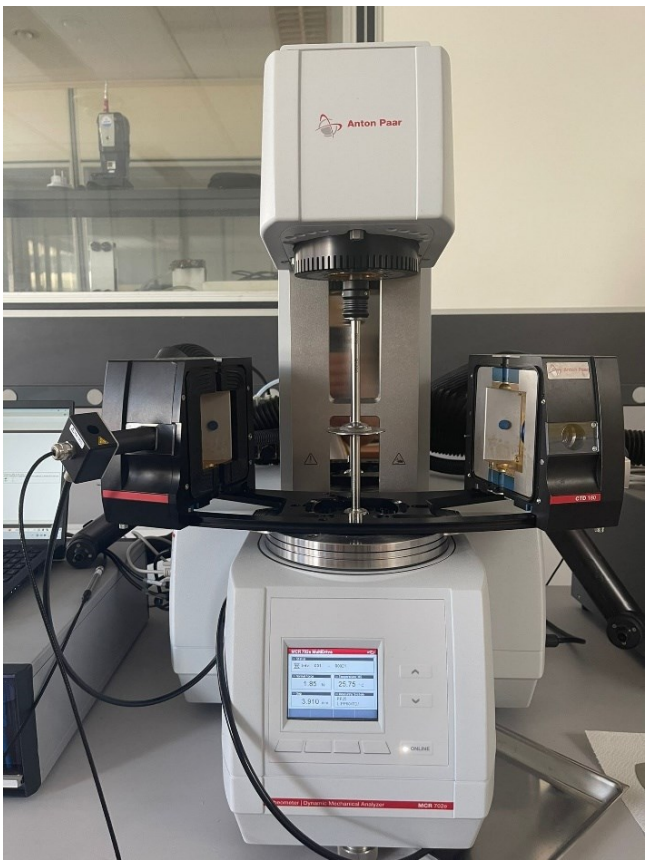

Fig.12: MCR 702e Anton-Paar rheometer

2.10 Field Emission Scanning Electron Microscopy (FE-SEM)

The microstructure of hydrogel constructs has been investigated using FE-SEM ZEISS SUPRA 40 (Zeiss, Oberkochen, DE) from UNIVPM SIMAU Department and FE_SEM ZEISS SUPRA 25 from UNIPG (Terni). Images were taken at magnitude 10.00K and 20.00K X. Both the hydrogels were mixed with DMEM-F12 high glucose (representative of cells) and compared to commercial bioink (CELLINK BIOINK®, CELLINK Gothenburg, Sweden) with and without cell suspension.

The inclusion procedure for SEM visualization of the samples is reported below.

1. Fix the samples in gluta-para (2%) overnight

2. Dilute 1:1 with phosphate buffer (PBS)

3. Wash with phosphate buffer for 15 min at RT

4. Post-fixation in 1% osmium tetroxide in phosphate buffer at 4°C for 1 hour

5. Wash with phosphate buffer for 15 min at RT

6. Dehydrate in EtOH at different concentrations (20, 50, 70, 80, 95 %)

7. Insert the samples into the filter paper sachets and place them in a beaker with 100% EtOH (4x15 min EtOH)

8. Dry the samples using Critical Point Drying (CPD) with hexamethyldisilane (HMDS) (Sigma-Aldrich, Gillingham, UK)

9. Mount the samples on aluminum stubs with graphite-based glue or with self-adhesive carbon discs (depending on the morphology of the sample) and store them in a small box (with silica gel) in a non-humid (dry) place.

10. Samples on aluminum stubs are sputter-coated whit gold before the visualization.

2.11 Optical Microscopy

To observe and count the spheroids, the images were acquired using the phase contrast optical microscope by Nikon (Nikon Europe, Amstelveen, The Netherlands) at times from 0 to 144h.

2.12 Dapi Staining

For DAPI staining, sterile PBS (Corning) was used in order to dilute the 4′,6-diamidino-2-phenylindole (DAPI) solution (ThermoFischer) to the final concentration of 300 nM. First of all, the scaffolds containing the spheroids were washed 1–3 times with sterile PBS and then were coated with the fluorescent dye solution of DAPI (300 nM) and incubated for 1–5 min, protected from light. Finally, the solution was removed by washing 2–3 times with PBS and images were acquired by using a Nikon fluorescent phase contrast light microscope.

2.13 Haematoxylin and Eosin Staining

Scaffolds were fixed in a 4% paraformaldehyde solution (Sigma-Aldrich, Merk, Darmstadt, Germany) and then embedded in paraffin. To prepare the paraffin sections, rehydration was carried out using xylene and a series of ethanol solutions with gradually decreasing concentrations. After washing with 50% ethanol, the sections were placed in distilled water for five minutes. The sections were then stained with haematoxylin (Bio-Optica, Milan, Italy) for two minutes, followed by rinsing in distilled water, and subsequently stained with Eosin (Bio-Optica) for two minutes. Another distilled water rinse followed the staining. The samples were then dehydrated through a graded ethanol series in ascending concentrations, treated with xylene, and finally mounted using Eukitt mounting solution (Orsatec GmbH, Kindler GmbH and Co., Bobingen, Germany).

3 Results

In this section, we present the comprehensive analyses performed on the formulated hydrogels suitable for bioink development. Each hydrogel underwent a series of evaluations to assess key factors such as structural integrity, rheological properties, and storage stability. These analyses allowed us to identify the most promising hydrogels for cell-laden bio fabrication, particularly in supporting the adhesion and proliferation of leiomyosarcoma cells. These results enabled us to outline the most stable and biocompatible hydrogel formulations, the 10% (w/v) alginate, as the most reliable candidate for further bioinks development (Fig.12). In a second phase, the selected hydrogels were combined with the leiomyosarcoma cells to form the bioinks, which were then subjected to cell adhesion and proliferation assays. The results were compared with a commercially available bioink (Cellink+ Bioink) used as a control to evaluate the performance of our formulations: although different printing pressures and other parameters were required depending on the specific bioink and day-print condition, the bioink formed with 10%(w/v) alginate hydrogel demonstrated excellent printability, successfully producing long-lasting 3D structures. The observed behavior during printing closely mirrored that of the Cellink bioink benchmark, emphasizing the strength and reliability of the hydrogels developed in this study. Furthermore, cellular adhesion and replication were assessed using DAPI staining, haematoxylin and eosin (H&E) staining, and optical microscopy, all of which yielded promising results. These analyses confirmed good cell viability, adhesion, and proliferation, with the behavior of the cells in the experimental bioinks mimicking that seen in the commercial bioink. This similarity in performance underscores their potential as viable, cost-effective alternatives for bioprinting applications. The following sub-paragraphs will detail the results of each analysis, highlighting the hydrogel that demonstrated the highest potential in the bioprinting process and their efficacy in supporting cellular behavior.

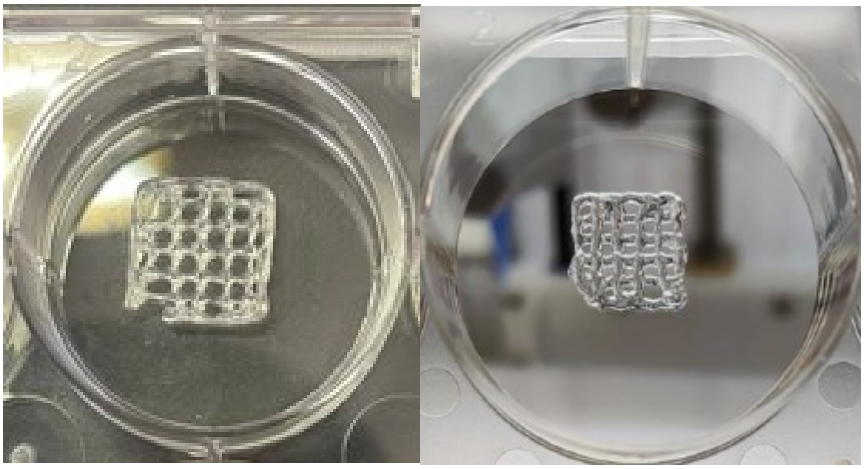

Fig.12: comparison of our 10% alginate scaffold (left) and commercial Cellink+ bioink (right)

3.1 Printability and Parameter Tuning

Our experience with 3D printing allowed us to identify the most print-friendly hydrogels by tuning the pressure, extrusion speed, and nozzle parameters for each formulation. Through these observations, the two most promising hydrogels in terms of printability were the 10% w/v alginate hydrogel and the 8% w/v alginate. These formulations demonstrated excellent extrusion characteristics, consistent layer stacking, and retained structural integrity post-printing. Their behavior during the printing process indicated optimal viscosity and flow, making them highly suitable for scaffold fabrication. Other formulations, while functional, exhibited challenges such as nozzle clogging, enhanced bubbles formation, irregular flow, or less precise layer resolution, especially when printing more intricate geometries (Fig.13).

Figure 14 presents the structural integrity of the 10%(w/v) alginate scaffold containing cells after one week of incubation. The scaffold was placed in an incubator to promote cell growth and scaffold maturation under controlled conditions. As shown in the image, the alginate scaffold maintained its original shape and structure throughout the incubation period, demonstrating its stability and resistance to degradation. This result underscores the suitability of the 10% alginate composition for creating robust, biocompatible scaffolds capable of supporting cell growth while retaining their form over time. The ability of the scaffold to maintain structural integrity is crucial for ensuring consistent cellular proliferation and tissue development.

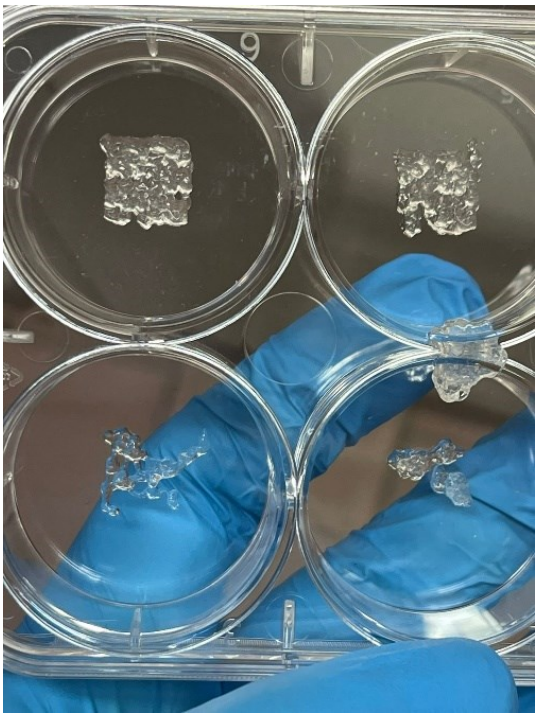

Fig.13: Failed geometries due to enhanced bobble formation and nozzle clogging

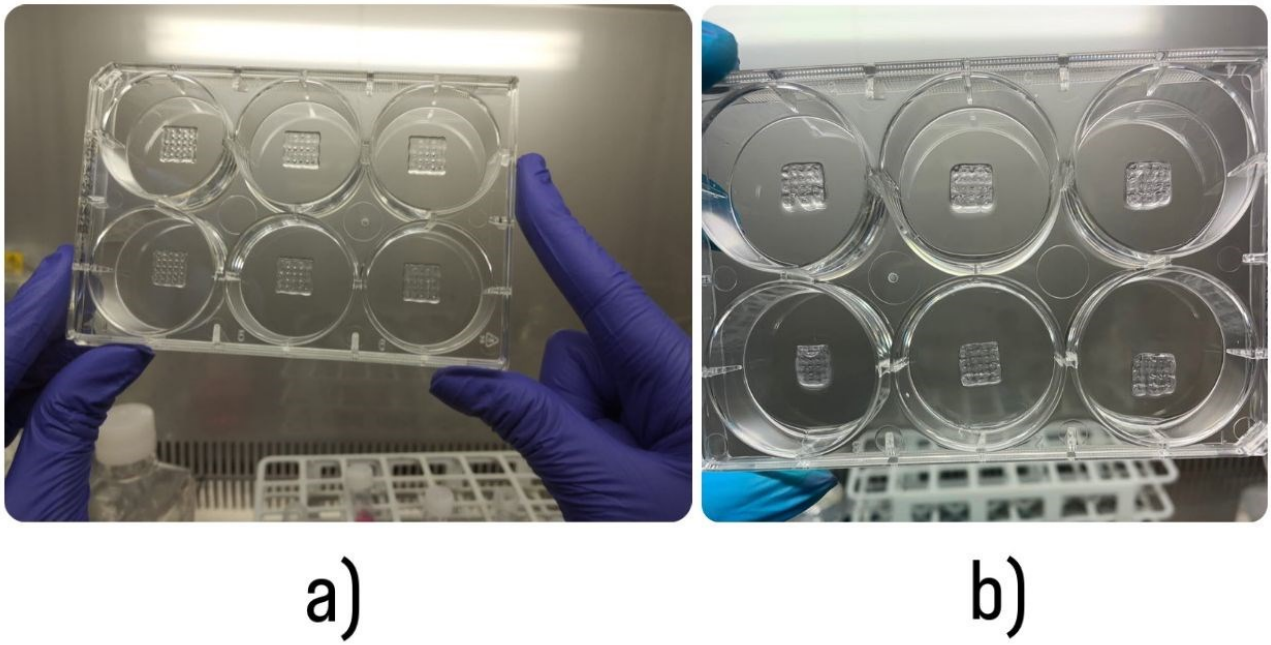

Fig.14: a) freshly printed 10% alginate bioinks scaffolds, b) bioinks scaffolds after one week of incubation

3.2 Morphological analysis (SEM)

The morphological structures of alginate-based (10 w/v %) hydrogels were examined using FE-SEM and subsequently compared with SEM images of CELLINK BIOINK. The detailed results are presented below for the plain matrix and for the cell-loaded ones. The proposed hydrogels exhibited a relatively smooth surface (Fig. 15c), without exhibiting any porous structure at a low magnification. In contrast, the commercial Cellink hydrogel displayed a wrinkled and porous architecture (Fig.15a,b). While the X10.00K magnification images portrayed a smoother surface, the X20.00 K images distinctly revealed a three-dimensional network structure and a more wrinkled morphology for the hydrogel proposed in this study (Fig.15d). This observation suggests favorable cell adhesion in situ, which can contribute to enhanced cell proliferation. However, while this morphology supports cell adhesion, it does not achieve the same level of cell attachment or proliferation observed with the commercial Cellink bioink, indicating that the bioink's surface features provide more optimal conditions for cell growth.

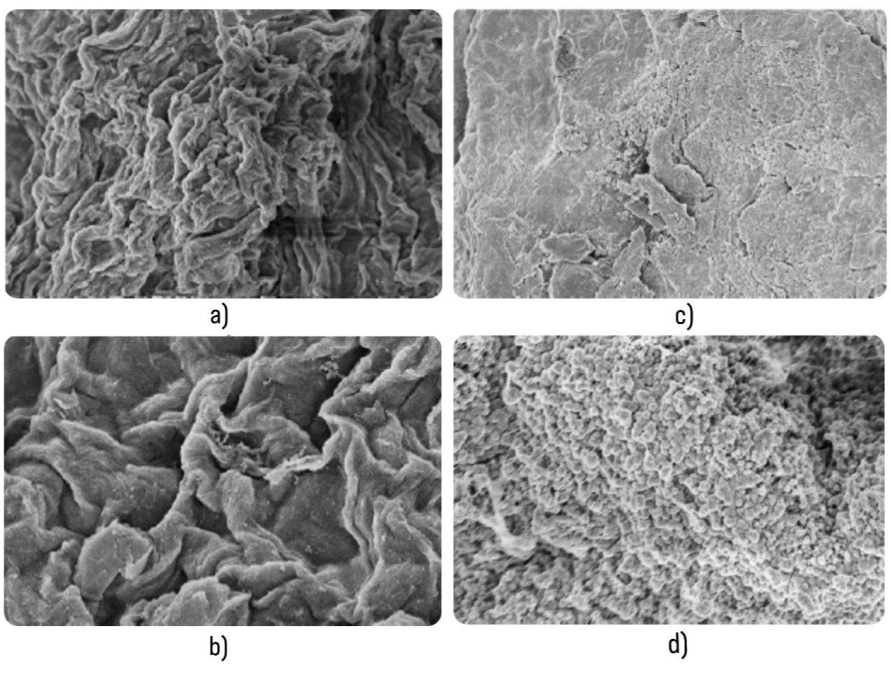

Figure 15: SEM micrographs showing the structural comparison of pure matrix between the commercial Cellink bioink (a,b) and our 10% (w/v) alginate bioink (c,d). Subplots (a) and (b) display Cellink bioink at magnifications of x10.00k and x20.00k, respectively. Subplots (c) and (d) show the same magnifications for the 10% (w/v) alginate bioink.

Figure 16 e 17 presents representative images of the cellink+ bioink and the alginate scaffold both loaded with leiomyosarcoma cells, where the presence of subcellular structures is evident (black arrowhead on Fig.17). Although small, these structures resemble mitochondria, a feature also observed in the commercial matrix, as indicated by the white arrowhead (Fig.16). These structures were captured at various magnifications for clearer visualization. Additionally, for the alginate 10%, spheroid's surface shows fine fibrils which may suggest the presence of collagen fibers, as marked by the blue arrowhead. Notably, this observation is consistent with the SEM analysis of the pure matrix, where the two scaffolds exhibit distinct structural characteristics (Fig.15). The 10% (w/v) alginate hydrogel demonstrates a relatively smooth and less porous surface, while the commercial Cellink bioink shows a more wrinkled and porous architecture. In summary, the FE-SEM analysis highlights the presence of cellular, subcellular, and extracellular structures within both bioinks, illustrating how each scaffold's microarchitecture supports cellular interaction and growth.

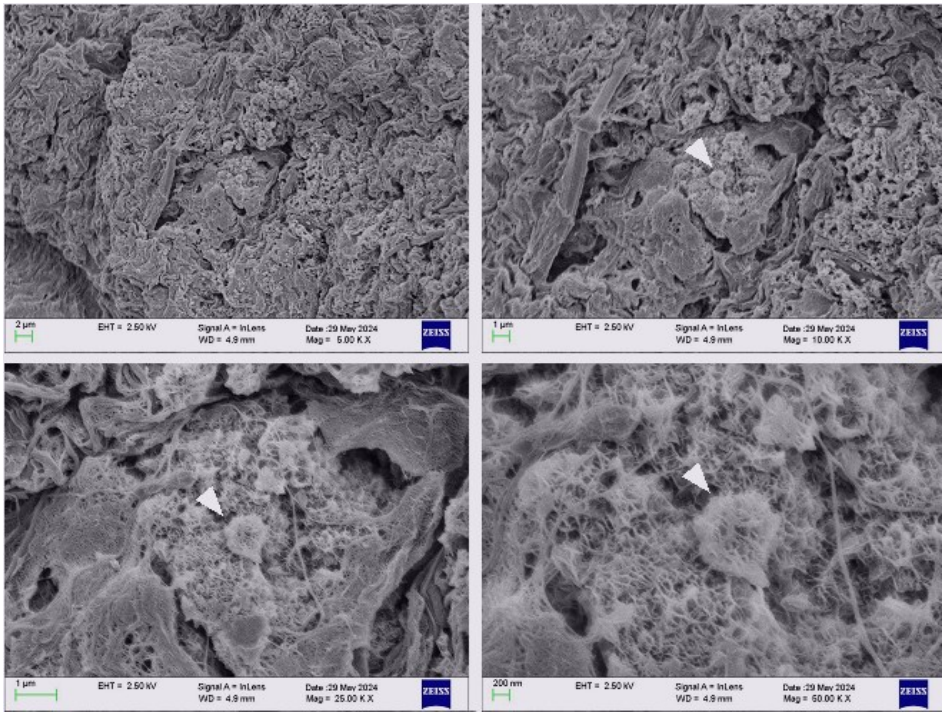

Fig.16: FE-SEM morphological investigation. Images of Cellink bioink alginate at different magnifications. The images show the presence of a biological structure indicated with the white arrowhead at different magnifications (5.00K X, 10.00K X, 25.00K X and 60.00K X).

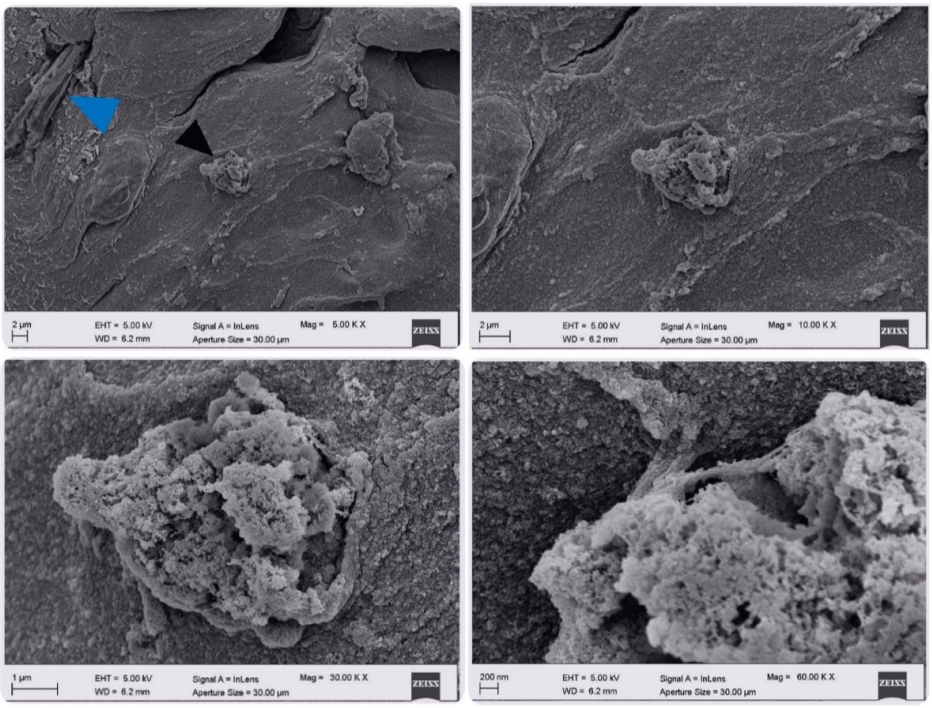

Fig.17: Morphological investigation FE-SEM. Images of alginate (10% w/v). The images show the presence of biological structure at different magnifications (5.00K X, 10.00K X, 30.00K X and 60.00K X).

3.3 Rheological analysis

During the bioprinting of hydrogel, the bioink is initially in a resting state within the cartridge, when exposed to the applied force, the bioink undergoes the transition to deform and flow in shear conditions when passing the nozzle wall. Subsequently, it obtains a new shape and eventually reaches a new resting state [34]. Key rheological properties associated with this process include viscosity, yield stress, viscoelastic shear moduli, and elastic recovery. The viscosity of bioinks represents the degree of resistance they exhibit to flow under applied stress. Several key factors influence this property, including (i) temperature, (ii) the composition and concentration of the bioink, and (iii) molecular weight and interaction of its components [35]. Viscosity significantly impacts the printability and shape fidelity of bioinks during 3D bioprinting [36]. In general, higher viscosity enhances printing resolution and ensures better shape fidelity, but it also increases shear stress during extrusion. This can negatively affect cell viability and compromise the biological functionality of the printed constructs [37]. To mitigate cell injury from high shear stress during bioprinting, several approaches can be employed, such as adjusting the printing pressure and speed or using nozzles with various geometries and sizes [38]. In the case of alginate bioinks, their unique behavior helps address this issue effectively. Alginate, with its anionic properties, allows the bioink to be extruded at a lower pressure, minimizing the shear stress experienced by cells. This is crucial for maintaining cell viability during the printing process. Immediately after extrusion, alginate undergoes ionic crosslinking when exposed to calcium ions, allowing the printed structure to solidify without requiring high pressure during extrusion. This approach not only reduces the risk of nozzle clogging but also ensures cell survival by limiting the maximum shear stress [39]. By crosslinking after extrusion, the alginate bioink achieves good structural stability while avoiding the drawbacks of low viscosity bioinks, such as poor resolution or instability.

Figure 18 shows the dependence of the viscoelastic parameters (G′ (Figure 18 a), G″ (Figure 18b) and tanδ Figure 18 c) as a function of oscillation frequency while the viscosity was studied as function of shear rate ($\dot{\gamma}$) (Figure 18 d)) for bioink and Alginate based formulations. Table 4 summarizes the rheological parameters of the different formulations at 25 °C processing temperature.

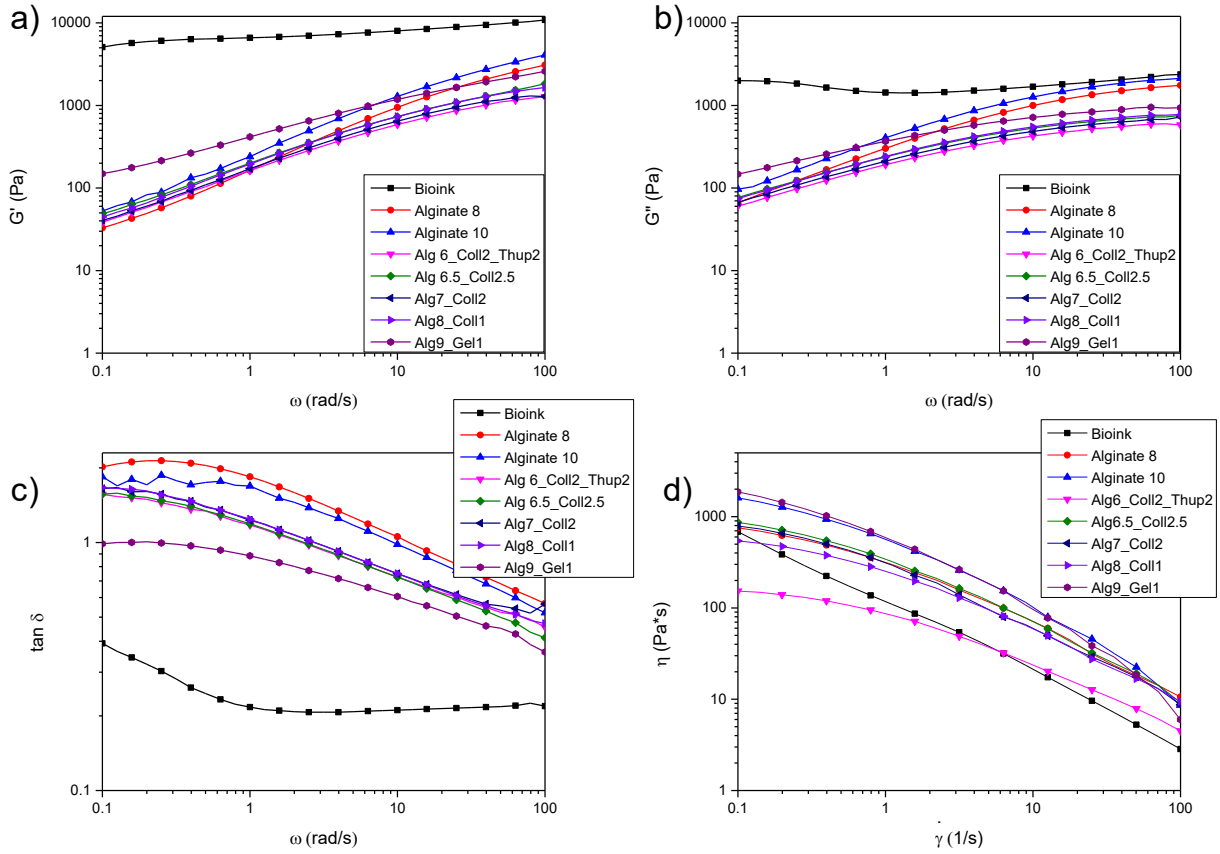

Figure 18: Variation of G′ (a), G″ (b), tanδ (c) as a function of ω and viscosity as function of shear rate ($\dot{\gamma}$) for Bioink and Alginate based gels.

Figure 19 shows the comparison of G′ and G′ ′ as a function of ω for Bioink and alginate-based systems. For Bionk and Alginate 9_Gel 1 the storage/elastic modulus (G′) (**Figure 18a)** presents higher values as compared with the loss/viscous modulus (G″) (**Figure 18b)**) (see also **Figure 19**) for each value of frequency. Therefore, the loss tangent values are less than unity for bionk and Alg9_Gel1 (**Figure 18c)**. Bioink and Alg9_Gel1 are solid-like biomaterial formulations (G'>G") (**Figure 19**) throughout the frequency scan. The other based systems are a non-Newtonian fluid showing liquid-like behaviour (G">G' and tanδ>1) and solid-like (G'>G" tanδ<1) behaviour as consequence of angular frequency values (**Table 4**).

Polymer-based systems with liquid behaviour are not considered suitable for the extrusion bioprinting process because they are unable to maintain their shape and size after extrusion and tend to change over time [40]. This disadvantage can be reduced or overcome using immediately after the extrusion process a cross-linker, the treatment favourites the crosslinking process in polymeric scaffolds. In this research activity, according to the literature, calcium chloride was used as cross-linker agent after the extrusion process of alginate-based materials [41]. The use of $CaCl_2$ improves the mechanical resistance, particularly tensile and compression strength, due to a crosslinking reaction between Ca^{2+} ions and carboxyl groups of sodium alginate [41]. Alginate_10 is solid-like for a wider of angular frequency values than Alginate_8 (9 rad/s <ω<100 rad/s and 13.5 rad/s <ω<100 rad/s, respectively). while for the other formulations solid-like behaviour is highlighted for 2.5 rad/s <ω<100 rad/s.

The bio-based polymeric formulations show non-Newtonian behaviour, the apparent viscosity (η) is dependent on shear rate ($\dot{\gamma}$) as reported in **Figure 18d.** By increasing the shear rates, the shear-thinning behaviour is observed, when the viscosity value is influenced by shear rate. The values of shear-thinning influence the different printable inks [42]. The impact of the different components and concentrations on rheological behaviour with respect to the shear rate determined a variation of viscosity characteristics. As the viscosity decreases with increasing the shear rate, all the formulations have shear thinning characteristics [43].

The gels can be extruded for shear stress values above yield stress, σ_y (**Table 4**) when the viscosity rapidly decreases, and the material starts to flow. The value of yield stress mainly reveals the resistance of the fluid to flow during the extrusion process, additionally this value is also directly correlated to the gel strength required to support subsequent 3D printed layers [44].

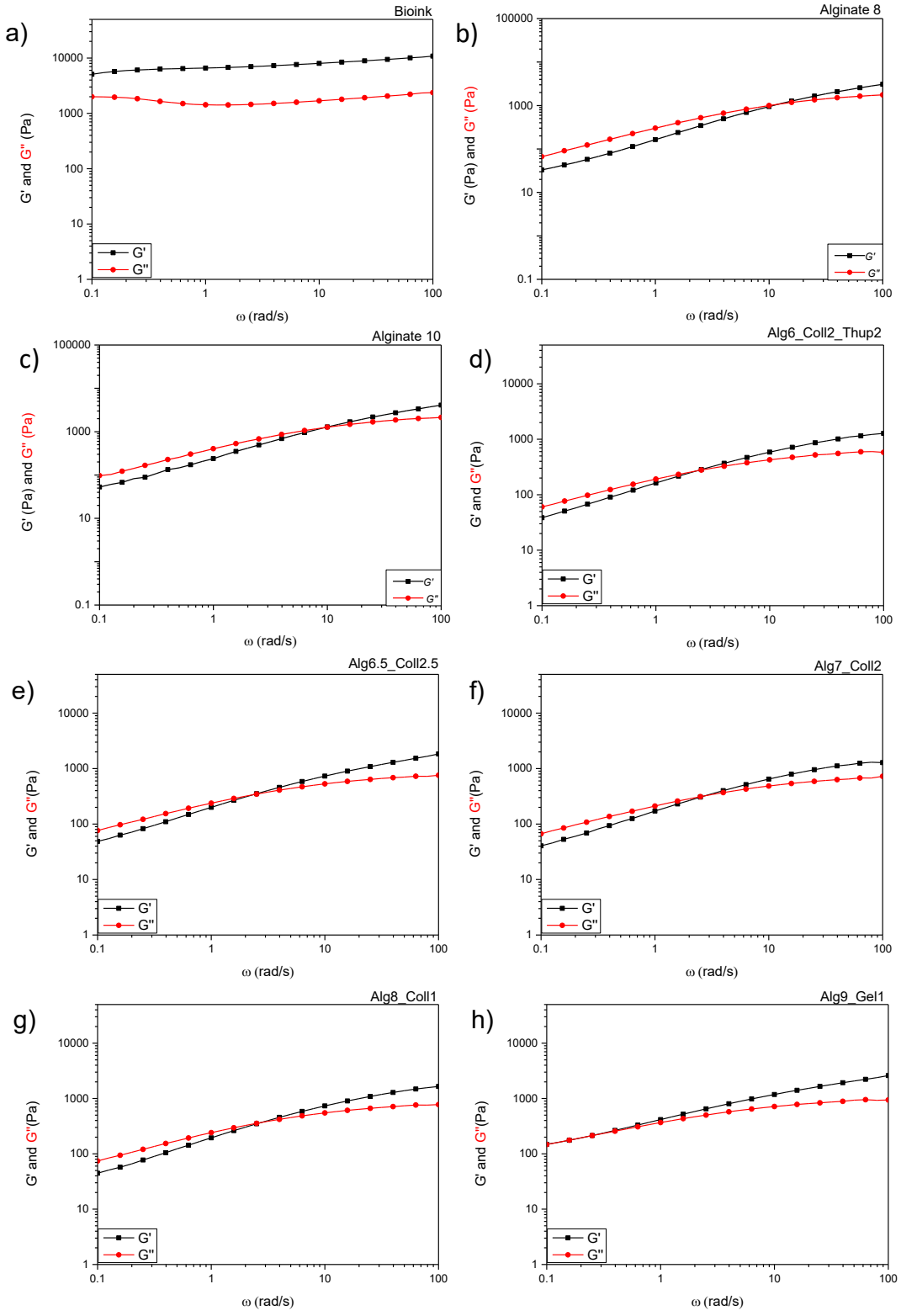

Figure 19: Comparison of G′ and G′ ′ as a function of ω for Bioink (**a**), Alginate 8 (**b**), Alginate 10 (**c**), Alg6_Coll2_Thup2 (**d**), Alg6.5_Coll2.5 (**e**), Alg6.5_Coll2.5 (**e**), Alg7_Coll2 (**f**), Alg8_Coll1 (**g**), Alg9_Gell1 (**g**) based gels.

Table 4: Rheological characteristics of the gels at 25 °C.

Formulations	G' (Pa) @ 1 rad/s	G" (Pa) @ 1 rad/s	G' (Pa) @ 100 rad/s	G" (Pa) 100 rad/s	σ_y (Pa)	η_y (Pa*s)
Bioink	6598	1431	10851	2376	73	515
Alginate 8	164	302	3086	1753	76	533
Alginate 10	240	405	4088	2129	161	1303
Alg6_Coll2_Thup2	163	192	1276	581	15	153
Alg6.5_Coll2.5	200	238	1837	759	86	864
Alg7_Coll2	171	211	1283	725	79	790
Alg8_Coll1	195	242	1652	778	54	393
Alg9_Gel1	416	368	2594	939	187	1867

G′ and G″ values at 1 rad/s and 100 rad/s were considered.

σ_y - yield stress.

η_y - the viscosity corresponding to σ_y.

3.4 Optical microscopy

Optical microscopy analysis was conducted during a week at 24, 48, 120 and 144 hours to monitor cell proliferation within the scaffolds made from the tested gels. At the 24-hour mark, microscopy provided an initial view of cell distribution within the substrate, offering a baseline for later comparisons, as depicted in Figure 20.

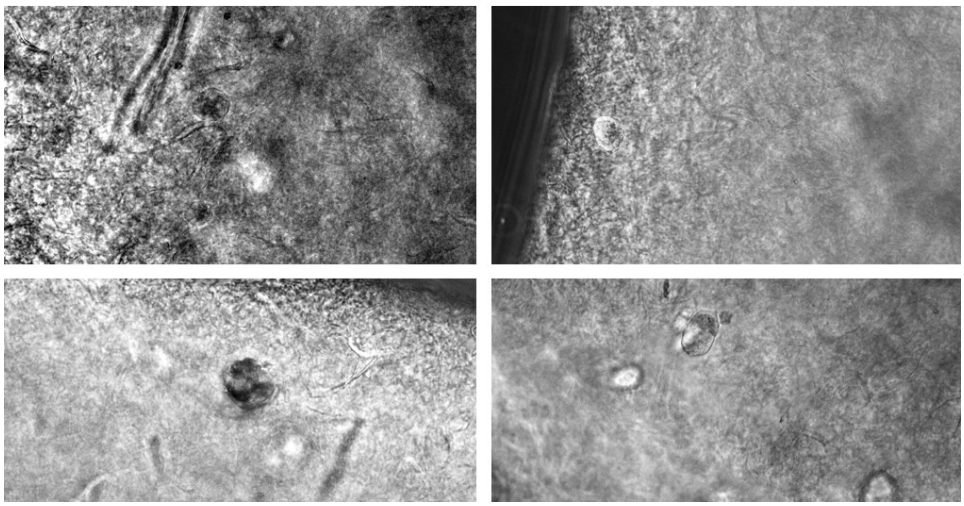

Fig.20: Optical microscope photographs (with x20 objective) of alginate (10% w/v) scaffold after 24h.

At 48 hours, a noticeable increase in cell density was observed. Figure 21 illustrates the formation of spheroids within the gel, suggesting that the cells were responding favorably to the environment. This increase in cell aggregation indicates that the gels provided a supportive matrix for cell growth.

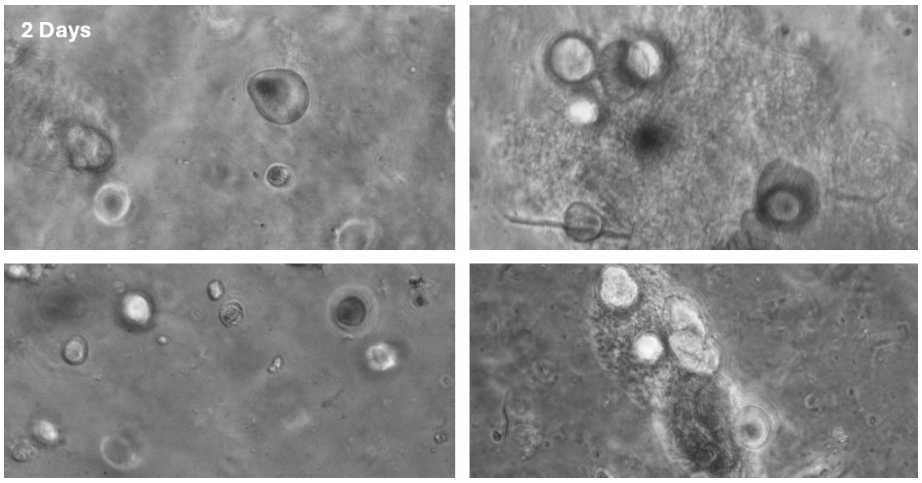

Fig.21: Optical microscope photographs (with x20 objective) of alginate (10% w/v) scaffold after 48h.

By 120 hours, further growth and development of the spheroids were seen, as shown in Figure 22. While the number of spheroids remained relatively stable, their size continued to increase, providing additional evidence of the scaffold's ability to support cell proliferation and aggregation over time.

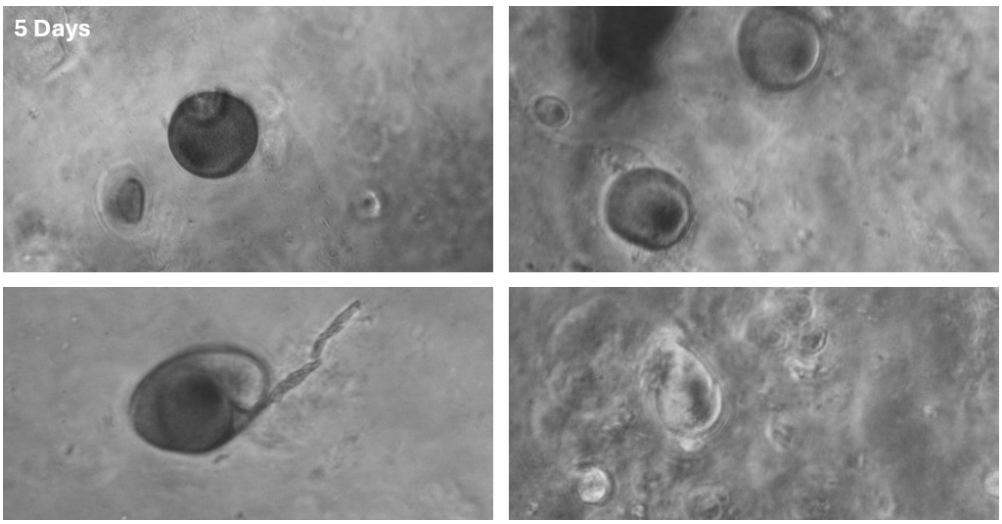

Fig.22: Optical microscope photographs (with x20 objective) of alginate (10% w/v) scaffold after 120h.

After 6 days (144 hours), the positive trend in spheroid size continued, as depicted in Figure 23. Although the number of spheroids did not significantly change, the noticeable expansion in their size demonstrates the scaffold's sustained capacity to promote cellular growth and aggregation, confirming its effectiveness as a viable platform for long-term spheroid development.

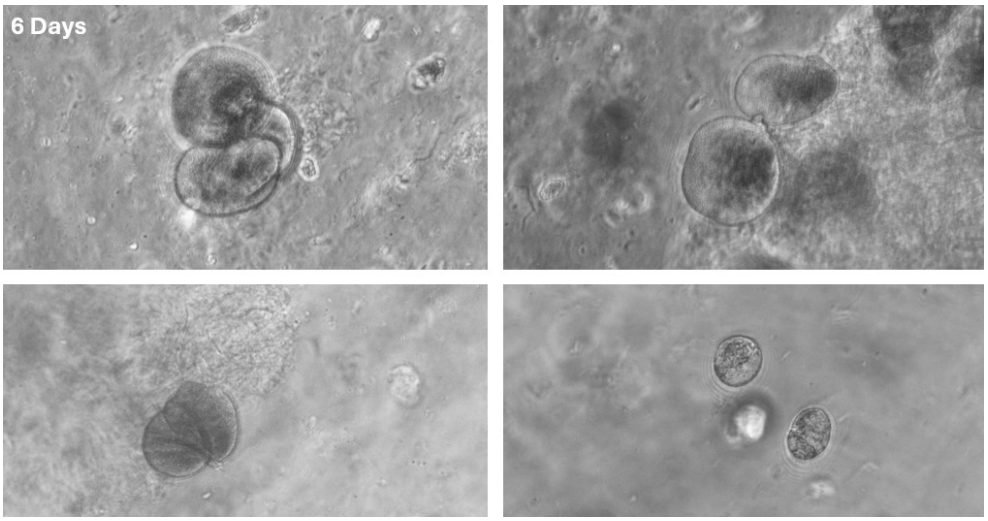

Fig.23: Optical microscope photographs (with x20 objective) of alginate (10% w/v) scaffold after 144h.

Figure 24 presents a detailed quantitative analysis of spheroid formation and growth within the 10% alginate scaffold over a period of 6 days, reflecting observations made through optical microscopy. The upper left graph shows the average number of spheroids per well (N=6), while the lower left bar chart represents the total spheroid count across multiple images. These graphs illustrate that although the number of spheroids stabilizes after day 2, their presence remains consistent over time. The two graphs on the right quantify the area of the spheroids, indicating a progressive increase in their size, which corroborates the optical microscopy findings. This suggests that while the number of spheroids does not dramatically increase, the cells continue to aggregate and grow, forming larger spheroids as the experiment progresses. Together, these graphs confirm the scaffold's effectiveness in promoting cell proliferation and spheroid expansion over time.

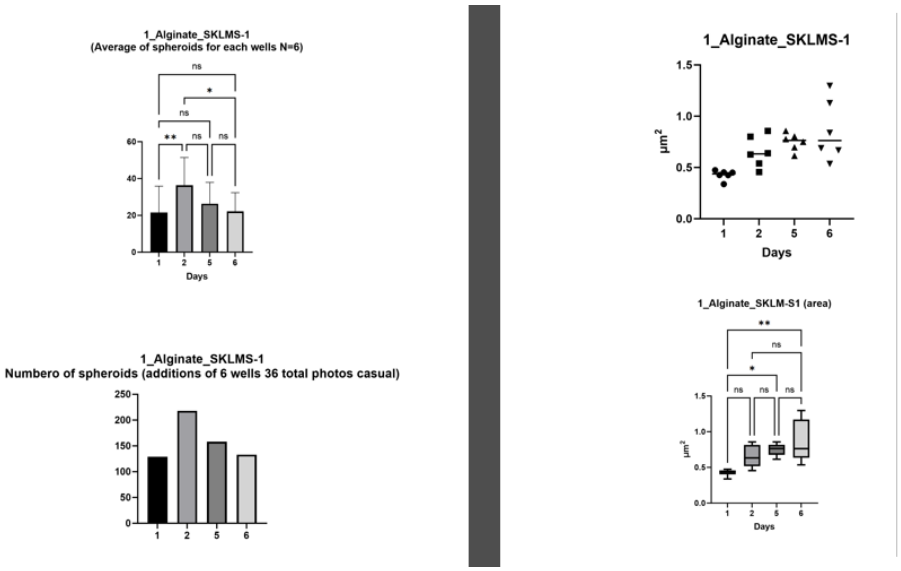

Fig.24: Statistical analysis of cell spheroid growth and development (spheroid's number and area) over time in alginate scaffold (N=6)

3.5 DAPI analysis

Cell growth analysis was further refined with the use of DAPI staining, which provided more precise insights into cell viability. Observations enabled accurate detection of cell presence and activity within the scaffold. DAPI staining specifically highlighted the nuclei of the cells, clearly confirming their viability at these stages and their number in the spheroids (Fig.25). The combination of visual observation of DAPI and hematoxylin/eosin (Fig.26) staining added a crucial layer of detail to understanding the cell growth dynamics. This allowed for the detailed detection of cell presence and activity, providing an in-depth view of the morphology in the bioinks studied. The fluorescence highlighted by DAPI allowed the nucleus of the cells to be clearly identified, helping to confirm their viability and cellular health within the bioinks.

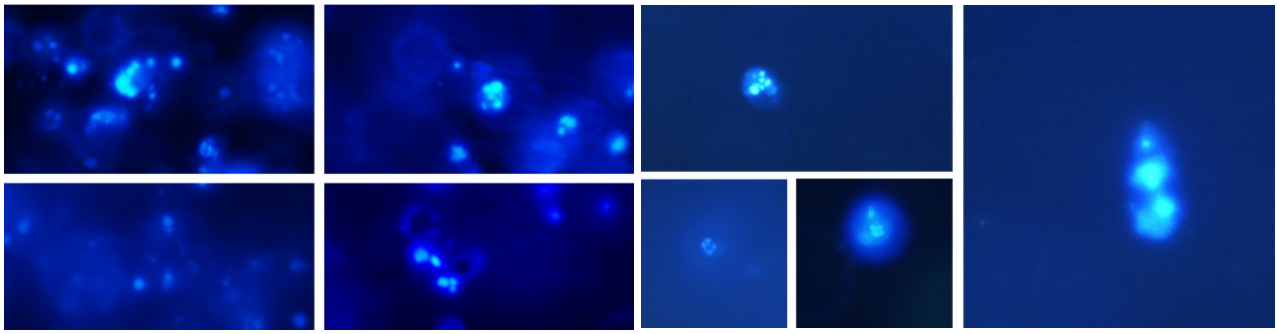

Fig.25: Images of spheroid'nuclei with DAPI staining. The images show spheroid in alginate scaffold after 48h.

3.6 Haematoxylin and Eosin Staining

Further analysis of the scaffolds was conducted using haematoxylin and eosin (H&E) staining, followed by examination under an optical microscope. Haematoxylin, a blue-purple dye, binds to nucleic acids, marking the cell nuclei, while eosin imparts a pink hue to proteins. This combination allows for clear visualization of tissue architecture: nuclei appear blue, while the cytoplasm and extracellular matrix vary in shades of pink. Well-preserved cells display detailed nuclear structures, and if numerous polyribosomes are present, the cytoplasm takes on a bluish tint. Additionally, the Golgi apparatus may be identified by a lighter region near the nucleus. From this staining procedure, abundant structural insights were revealed, showing that each spheroid within the matrices contained multiple cells, highlighting their multicellular composition. Figure 26 shows results from DAPI and H&S staining for commercial grade Cellink+ bioink and our 10%(w/v) alginate bioink.

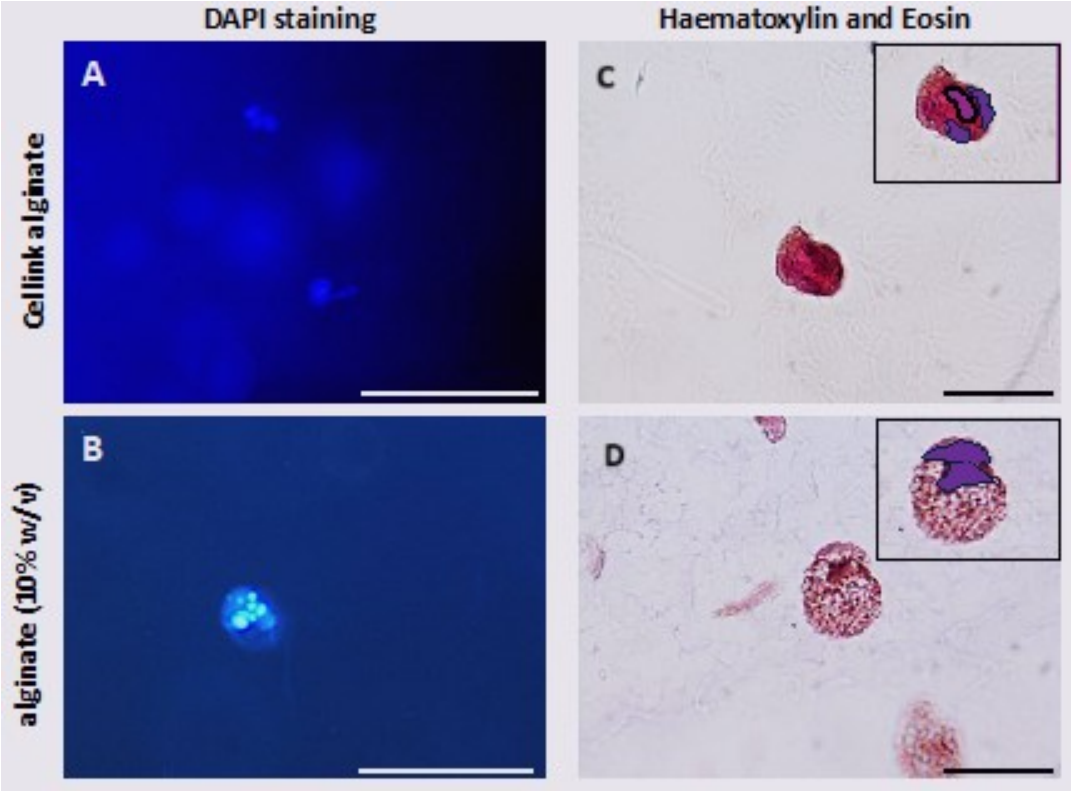

Fig. 26: DAPI fluorescent staining of Cellink Bioink (A) and alginate (10% w/v) (B). Haematoxylin and eosin images of Cellink Bioink (C) and alginate (10% w/v) (D)

4 Discussion & Conclusion

The results of this study have identified 10% w/v alginate as the most effective construct for maintaining structural integrity over a period of 6 days. This formulation demonstrated superior resistance to mold and bacterial growth, as well as promoting significant cellular adhesion and proliferation. These findings were supported by a combination of microscopic, rheometric, and storage control analyses, highlighting its potential as a reliable scaffold material for bioprinting applications.

From the rheological data, alginate-based systems display both liquid-like and solid-like behaviors, which are typically unsuitable for extrusion-based bioprinting. However, this limitation can be effectively addressed by introducing a crosslinker immediately after the extrusion process, stabilizing the structure and ensuring successful printing. Additionally, with this process, we can print the bioink with lower pressures and make a safer environment for the loaded cells. Scanning electron microscopy (SEM) studies revealed that the proposed hydrogel exhibits a three-dimensional network structure with a wrinkled morphology, emphasizing its potential to support complex cellular interactions and foster the formation of biomimetic tissues. However, the performance of the developed hydrogel is slightly less robust compared to the commercial Cellink bioink. The porous structure that is prominent in the commercial bioink only appears at deeper magnifications for the 10% alginate hydrogel. This indicates that while both bioinks can support cellular adhesion and interaction, the commercial bioink's surface architecture, with more evident porosity, is more conducive to cellular proliferation. Observation of cell proliferation and spheroids aggregation through the inverted microscope provided crucial insights into cellular behavior. Images captured at 24, 48, 120 and 144 hours (6 days) revealed a progressive and consistent increase in cell presence, demonstrating the effectiveness of the bioink in promoting cell viability and proliferation over time. The analysis also showed a clear trend of cell proliferation and spheroid aggregation concorded with statistical analysis, further indicating favorable conditions for cellular interaction and growth within the hydrogel matrices. The use of DAPI staining in this study was essential for highlighting the nuclei of the cells within the spheroids, providing a clear representation of cell distribution and organization. The fluorescence from DAPI enabled the precise identification of multiple nuclei per spheroid, which is a positive indicator of successful cellular proliferation and spheroid formation which is necessary for effective tissue formation. Furthermore, the DAPI results were compared with those obtained from Hematoxylin and Eosin (H&E) staining to provide a more comprehensive understanding and visualization of the nuclei within the spheroids. This combination of techniques allowed for clearer distinction and confirmation of the nuclei, offering detailed insight into the cellular organization for

both the commercial-grade Cellink+ bioink and the 10% (w/v) alginate bioink. The integration of these staining methods supports the evaluation of cell distribution and proliferation across the scaffolds, further solidifying the comparative analysis of the bioinks performance.

This study provides important insights into the development of low-cost, biocompatible scaffolds for 3D bioprinting. By utilizing accessible materials such as sodium alginate, gelatin, and xanthan gum, we have demonstrated that it is possible to create bioinks that perform well in terms of structural stability and cellular compatibility. The use of 10% w/v alginate proved effective for supporting cellular adhesion and replication, making it a promising candidate for scalable bioprinting applications. However, while the alginate-based bioink shows promising results, it does not yet match the superior performance of commercial bioinks, particularly in terms of the complex cellular interactions and porosity observed in the Cellink+ bioink. It is important to note that this is an initial study, and further analysis is needed to refine and optimize the alginate bioink for more advanced applications. Nevertheless, our results offer a solid foundation for future developments in the field of 3D bioprinting.

One of the key advantages of our proposed hydrogel is its cost-effectiveness. When compared to the commercial Cellink+ bioink, which costs approximately 1200 euros for 10 cartridges of 3 ml (30 ml total), our alginate-based bioink stands out as a significantly cheaper alternative. Based on our calculations, producing 10 cartridges (30 ml total) of the 10%(w/v) alginate bioink would cost around 150.51 euros, which can lead to a drastic reduction in price (Tab.5). This substantial cost difference, while maintaining high performance, demonstrates the potential for large-scale applications of this bioink in 3D bioprinting, offering a sustainable, accessible solution for both research and industrial applications.

Tab.5: Virtual production cost of 10 10%(w/v) alginate bioink cartridges of 3ml each comprehensive of 15ml CaCl2 flask.

Material	**Quantity**	**Unit Price**	**Total Cost**
Sodium alginate	3 g	€0.15	€0.45
Distilled water	30 ml	€0.002	€0.06
Empty 3 ml cartridges	10	€5.00	€50.00
Crosslinker ($CaCl_2$)	10 × 15 ml	€10.00	€100.00
Total Cost			**€150.51**

Future developments could focus on enhancing the mechanical properties of these hydrogels, particularly for load-bearing applications such as bone or cartilage regeneration. By refining the crosslinking techniques or incorporating additional materials such as hydroxyapatite or nanomaterials, it may be possible to increase the mechanical strength and durability of the scaffolds without compromising biocompatibility. Moreover, the integration of controlled-release systems within the scaffold matrix could enable the delivery of growth factors or other bioactive molecules, further enhancing tissue regeneration and healing processes.

In conclusion, the findings of this study not only validate the use of low-cost biopolymers for 3D bioprinting but also provide a framework for future research aimed at optimizing scaffold properties for a wide range of biomedical applications.

Bibliography

[1]. Jia J, Richards DJ, Pollard S, Tan Y, Rodriguez J, Visconti RP, Trusk TC, Yost MJ, Yao H, Markwald RR, Mei Y. Engineering alginate as bioink for bioprinting. Acta Biomater. 2014 Oct;10(10):4323-31. doi: 10.1016/j.actbio.2014.06.034. Epub 2014 Jul 1. PMID: 24998183; PMCID: PMC4350909.

[2]. Cohen DL, Malone E, Lipson H, Bonassar LJ. Direct freeform fabrication of seeded hydrogels in arbitrary geometries. Tissue Eng. 2006 May;12(5):1325-35. doi: 10.1089/ten.2006.12.1325. Erratum in: Tissue Eng. 2009 Oct;15(10):3211. PMID: 16771645.

[3]. Lee M, Wu BM. Recent advances in 3D printing of tissue engineering scaffolds. Methods Mol Biol. 2012;868:257-67. doi: 10.1007/978-1-61779-764-4_15. PMID: 22692615.

[4]. You F, Eames BF, Chen X. Application of Extrusion-Based Hydrogel Bioprinting for Cartilage Tissue Engineering. Int J Mol Sci. 2017 Jul 23;18(7):1597. doi: 10.3390/ijms18071597. PMID: 28737701; PMCID: PMC5536084.

[5]. Ertesvåg H. Alginate-modifying enzymes: biological roles and biotechnological uses. Front Microbiol. 2015 May 27;6:523. doi: 10.3389/fmicb.2015.00523. PMID: 26074905; PMCID: PMC4444821.

[6]. Bhattarai N., Li Z., Edmondson D., Zhang M. Alginate-Based Nanofibrous Scaffolds: Structural, Mechanical, and Biological Properties. Adv. Mater. 2006;18:1463–1467.

[7]. Zhang M., Zhao X. Alginate Hydrogel Dressings for Advanced Wound Management. Int. J. Biol. Macromol. 2020;162:1414–1428.

[8]. Ruvinov E., Cohen S. Alginate biomaterial for the treatment of myocardial infarction: Progress, translational strategies, and clinical outlook: From ocean algae to patient bedside. *Adv. Drug Deliv. Rev.* 2016;**96**:54–76.

[9]. Zhang H., Cheng J., Ao Q. Preparation of Alginate-Based Biomaterials and Their Applications in Biomedicine. *Mar. Drugs.* 2021;**19**:264.

[10]. Chen H., Xing X., Tan H., Jia Y., Zhou T., Chen Y., Ling Z., Hu X. Covalently antibacterial alginate-chitosan hydrogel dressing integrated gelatin microspheres containing tetracycline hydrochloride for wound healing. *Mater. Sci. Eng. C.* 2017;**70**:287–295.

[11]. Groll J, Boland T, Blunk T, Burdick JA, Cho DW, Dalton PD, Derby B, Forgacs G, Li Q, Mironov VA, Moroni L, Nakamura M, Shu W, Takeuchi S, Vozzi G, Woodfield TB, Xu T, Yoo JJ, Malda J. Biofabrication: reappraising the definition of an evolving field. Biofabrication. 2016 Jan 8;8(1):013001.

[12]. Zhang YS, Yue K, Aleman J, Moghaddam KM, Bakht SM, Yang J, Jia W, Dell'Erba V, Assawes P, Shin SR, Dokmeci MR, Oklu R, Khademhosseini A. 3D Bioprinting for Tissue and Organ Fabrication. Ann Biomed Eng. 2017 Jan;45(1):148-163.

[13]. Zhang YS, Duchamp M, Oklu R, Ellisen LW, Langer R, Khademhosseini A. Bioprinting the Cancer Microenvironment. ACS Biomater Sci Eng. 2016 Oct 10;2(10):1710-1721.

[14]. Kang HW, Lee SJ, Ko IK, Kengla C, Yoo JJ, Atala A. A 3D bioprinting system to produce human-scale tissue constructs with structural integrity. Nat Biotechnol. 2016 Mar;34(3):312-9.

[15]. Derakhshanfar S, Mbeleck R, Xu K, Zhang X, Zhong W, Xing M. 3D bioprinting for biomedical devices and tissue engineering: A review of recent trends and advances. Bioact Mater. 2018 Feb 20;3(2):144-156.

[16]. Lee HJ, Kim YB, Ahn SH, Lee JS, Jang CH, Yoon H, Chun W, Kim GH. A New Approach for Fabricating Collagen/ECM-Based Bioinks Using Preosteoblasts and Human Adipose Stem Cells. Adv Healthc Mater. 2015 Jun 24;4(9):1359-68.

[17]. Loo Y, Lakshmanan A, Ni M, Toh LL, Wang S, Hauser CA. Peptide Bioink: Self-Assembling Nanofibrous Scaffolds for Three-Dimensional Organotypic Cultures. Nano Lett. 2015 Oct 14;15(10):6919-25.

[18]. Lee DY, Lee H, Kim Y, Yoo SY, Chung WJ, Kim G. Phage as versatile nanoink for printing 3-D cell-laden scaffolds. Acta Biomater. 2016 Jan;29:112-124.

[19]. Maria Cristina Straccia, Giovanna Gomez d'Ayala, Ida Romano, Paola Laurienzo. Novel zinc alginate hydrogels prepared by internal setting method with intrinsic antibacterial activity, Carbohydrate Polymers, Volume 125, 2015, Pages 103-112, ISSN 0144-8617.

[20]. Cheng J., Jia Z., Li T. A constitutive model of microfiber reinforced anisotropic hydrogels: With applications to wood-based hydrogels. *J. Mech. Phys. Solids.* 2020;138:103893.

[21]. Echalier C., Valot L., Martinez J., Mehdi A., Subra G. Chemical cross-linking methods for cell encapsulation in hydrogels. *Mater. Today Commun.* 2019;20:100536.

[22]. Dodero A., Pianella L., Vicini S., Alloisio M., Ottonelli M., Castellano M. Alginate-based hydrogels prepared via ionic gelation: An experimental design approach to predict the crosslinking degree. *Eur. Polym. J.* 2019;118:586–594.

[23]. Zhou Q., Kang H., Bielec M., Wu X., Cheng Q., Wei W., Dai H. Influence of different divalent ions cross-linking sodium alginate-polyacrylamide hydrogels on antibacterial properties and wound healing. *Carbohydr. Polym.* 2018;197:292–304.

[24]. Netti F., et al. Stabilizing gelatin-based bioinks under physiological conditions by incorporation of ethylene-glycol-conjugated Fmoc-FF peptides. *Nanoscale.* 2022;14(23):8525–8533.

[25]. Bai X., et al. Fabrication of engineered heart tissue grafts from alginate/collagen barium composite microbeads. *Biomed. Mater.* 2011;6(4)

[26]. Meyer M. Processing of collagen based biomaterials and the resulting materials properties. *Biomed. Eng. Online.* 2019;18(1):1–74.

[27]. Li Z., Ruan C., Niu X. 2023. Collagen-based bioinks for regenerative medicine: fabrication, application and prospective. (Medicine in Novel Technology and Devices).

[28]. Amirrah I.N., et al. A comprehensive review on collagen type I development of biomaterials for tissue engineering: from biosynthesis to bioscaffold. *Biomedicines.* 2022;10(9):2307.

[29]. M. Kang, O. Oderinde, S. Liu, Q. Huang, W. Ma, F. Yao, G. Fu. Characterization of xanthan gum-based hydrogel with Fe ions coordination and its reversible sol-gel conversion. Carbohydr. Polym., 203 (2019), pp. 139-147,

[30]. V. Bueno, D. Petri. Xanthan hydrogel films: molecular conformation, charge density and protein carriers. Carbohydr. Polym., 101 (2014), pp. 897-904,

[31]. F. Ngwabebhoh, O. Zandraa, R. Patwa, N. Saha, Z. Capáková, P. Saha. Self-crosslinked chitosan/dialdehyde xanthan gum blended hypromellose hydrogel for the controlled delivery of ampicillin, minocycline and rifampicin. Int. J. Biol. Macromol., 167 (2021), pp. 1468-1478,

[32]. Y. Deng, M. Huang, D. Sun, Y. Hou, Y. Li, T. Dong, X. Wang, L. Zhang, W. Yang. Dual physically cross-linked κ-carrageenan-based double network hydrogels with superior self-healing performance for biomedical application. ACS Appl. Mater. Interfaces, 10 (43) (2018), pp.

[33]. A. Belloni, V. Notarstefano, S. Greco, P. Pellegrino, E. Giorgini, P.Ciarmela, FTIR Microspectroscopy as a new probe to study human uterine lesions: Characterization of tumor cell lines from uterine smooth muscle cells and evaluation of EPA and DHA in vitro treatments, Biochimica et Biophysica Acta (BBA) - Molecular Basis of Disease, Volume 1870, Issue 1, 2024

[34]. A. Schwab, R. Levato, M. D'Este, S. Piluso, D. Eglin, J. Malda. Printability and shape fidelity of bioinks in 3D bioprinting. Chem. Rev., 120 (2020), pp. 11028-11055

[35]. S. Bom, R. Ribeiro, H.M. Ribeiro, C. Santos, J. Marto. On the progress of hydrogel-based 3D printing: Correlating rheological properties with printing behaviour. Int. J, Pharm (2022), p. 121506

[36]. G.H. Yang , D. Kang, S. An, J.Y. Ryu, K. Lee, J.S. Kim, M.-Y. Song , Y.S. Kim, S.M. Kwon, W.-K. Jung, *et al.*. Advances in the development of tubular structures using extrusion-based 3D cell-printing technology for vascular tissue regenerative applications. Biomater. Res., 26 (2022), pp. 1-13

[37]. M.E. Cooke, D.H. Rosenzweig. The rheology of direct and suspended extrusion bioprinting. APL Bioeng., 5 (2021), p. 11502

[38]. A.A. Mohammed, M.S. Algahtani, M.Z. Ahmad, J. Ahmad. Optimization of semisolid extrusion (pressure-assisted microsyringe)-based 3D printing process for advanced drug delivery application. Ann. 3D Print. Med., 2 (2021), Article 100008

[39].L. Fischer, M. Nosratlo, K. Hast, E. Karakaya, N. Ströhlein, T.U. Esser, R. Gerum, S. Richter, F. Engel, R. Detsch, *et al.*. Calcium supplementation of bioinks reduces shear stress-induced cell damage during bioprinting. Biofabrication, 14 (2022), p. 45005

[40]. D. Wu, Y. Yu, J. Tan, L. Huang, B. Luo, L. Lu, C. Zhou 3D bioprinting of gellan gum and poly(ethylene glycol) diacrylate based hydrogels to produce human-scale constructs with high-fidelity Mater. Des., 160 (2018), pp. 486-495, 10.1016/j.matdes.2018.09.040; Nacu, Isabella, Maria Bercea, Loredana Elena Niță, Cătălina Anișoara Peptu, Maria Butnaru, and Liliana Vereștiuc. "3D bioprinted scaffolds based on functionalized gelatin for soft tissue engineering." Reactive and Functional Polymers (2023): 105636

[41]. Lu, Hao, Jonathan A. Butler, Nicole S. Britten, Prabhuraj D. Venkatraman, and Sameer S. Rahatekar. "Natural antimicrobial nano composite fibres manufactured from a combination of alginate and oregano essential oil." Nanomaterials 11, no. 8 (2021): 2062; Tabriz, Atabak Ghanizadeh, Miguel A. Hermida, Nicholas R. Leslie, and Wenmiao Shu. "Three-dimensional

bioprinting of complex cell laden alginate hydrogel structures." Biofabrication 7, no. 4 (2015): 045012.).

[42]. M. Bercea, Rheology as a tool for fine-tuning the properties of printable bioinspired gels, Molecules 28 (2023) 2766.

[43]. Habib, M. A., & Khoda, B. (2022). Rheological analysis of bio-ink for 3D bio-printing processes. Journal of manufacturing processes, 76, 708-718.

[44]. M.A. Sakr, K. Sakthivel, T. Hossain, S.R. Shin, S. Siddiqua, J. Kim, K. Kim, Recent trends in gelatin methacryloyl nanocomposite hydrogels for tissue engineering, J. Biomed. Mater. Res. A. 110 (2021) 708–724